International Journal of Thermophysics, Vol. 23, No. 5, September 2002 (© 2002)

Evolution of Near-Surface Elemental Composition Profile and Its Effect on Thermal Diffusivity[1]

Y. W. Kim[2]

In a series of recent experiments, utilizing the method of time resolved spectroscopy of laser-produced plasma (LPP) plumes from specimen surfaces, the near-surface elemental composition profiles were observed to be nonuniform and significantly different from the respective bulk composition. A new study of three alloy systems is reported, with a view toward establishing the causal relationship between the near-surface elemental composition profile of a specimen and its thermophysical properties in general and thermal diffusivity in particular. The systems in question are as follows: two-element Nichrome ribbon; four-element magnetic Mumetal foil; and four-element Wood's alloy. The method of LPP plume spectroscopy has been used throughout to successively expose new surface layers and measure the composition and thermal diffusivity. With two of the systems, modification of the near-surface elemental composition profiles has been forced. Sustained electrical heating of a Nichrome ribbon specimen revealed preferential diffusion of chromium to the surface, affecting the spectral emissivity and thermal diffusivity as well as depth-dependent local heating rates. In the case of Wood's alloy a sample is melted and re-solidified under a protocol that highlights gravitational forcing. The noncontact spectroscopic method has been used to discover that the top and bottom surfaces acquire two different composition profiles and exhibit commensurate disparity in the measured thermal diffusivity profiles.

KEY WORDS: depth-dependent; elemental composition profile; Mumetal; Nichrome; spectral emissivity; thermal diffusivity; Wood's alloy.

[1] Paper presented at the Sixth International Workshop on Subsecond Thermophysics, September 26–28, 2001, Leoben, Austria.

[2] Department of Physics, Lewis Laboratory #16, Lehigh University, Bethlehem, Pennsylvania 18015-3182. E-mail: ywk0@lehigh.edu

0195-928X/02/0900-1171/0 © 2002 Plenum Publishing Corporation

1. INTRODUCTION

Assembly of a set of disparate alloying elements into one multi-element alloy by pyrometallurgy is fundamentally a complex undertaking due to wide-ranged element-specific thermophysical properties, inter-elemental interactions, and the effects that are brought on them by the thermodynamics imposed by the ambient conditions. Especially, the time evolution of the thermal gradient imposed on the alloy system impacts strongly the final outcome of the three-dimensional composition profile. Some of the consequent prominent features, such as chemical segregation and formation of interlocking dendrites, profoundly affect the resulting alloy properties.

Of considerable interest has been the fact that there develops a surface composition profile, which is generally different from that in the interior of the bulk alloy material. Corrosion and coatings are two well-known examples, one a result of passive interactions with environmental conditions and the other an intentional surface modification. The effects range from large variations in spectral emissivity [1, 2] and corrosion and wear rates [3, 4] to depth-dependent thermophysical properties [5, 6]. Video-imaging studies of solidification of metallic alloys have indicated a hierarchy of surface segregation [7–9]. Element-specific diffusion, inter-elemental solubility and the buoyancy due to density disparity among constituent elemental matters [10–13] are the most prominent of the physics in the system. Container walls and trace-level impurity particles mediate nucleation of crystallites in the melt that are either difficult to eliminate, to control or even to quantify. In recent years, as a result, significant development has been realized in the area of containerless processing of molten alloys [2, 7–9, 14–17]. In the case of ground-based studies, fluid-dynamic, acoustic, or electromagnetic forces must now be addressed in the analysis, and their effects are demonstrated in some microgravity experiments [10, 15]. The problem of chemical separation can be explored more fundamentally by reducing the number of competing physical processes–namely, the role of gravity on the alloy melt undergoing solidification.

There has been a distinguished series of studies on quantitative understanding of the physical processes at play in solidification that are well documented in the literature. Some are in the form of analysis and numerical modeling [18–27], and others in detection and observation of certain aspects of solidification [15, 16, 28–30]. Many different binary alloy systems have been examined. In-process composition analysis, however, had been prominently absent until now. We are now in a unique position to introduce a new methodology into the study of chemical segregation [31–34]. The evolution of elemental composition near the free surface of an alloy specimen can be mapped either as a function of depth or across

the thermodynamic boundary of the melt-to-solid phase transition [5, 6]. This is necessary because, on a fundamental level, material composition dictates the thermophysical and topological properties of alloys.

Three different alloys have been examined: 80–20 nickel-chromium ribbon, four-element magnetic "Mumetal" alloy foil, and the four-element system of Wood's alloy. The depth dependence of the composition profile is determined by repeatedly ablating the free surface of the specimen by high power laser pulses and carrying out quantitative spectroscopy of the spectral emissions from each LPP plume. In the case of Wood's alloy the specimen has been taken through a prescribed sequence of melting and resolidification. Depth-resolved analysis has been carried out at both the top and bottom surfaces by laser-produced plasma plume spectroscopy.

2. BASIC APPROACH

The method is based on producing high-temperature, high-density plasma by means of a single high-power laser pulse incident on the specimen surface. When the criterion that the receding free surface be kept in pace with the thermal diffusion front propagating into the bulk during laser heating is satisfied, the LPP plume becomes representative of the specimen in its elemental composition [5, 35–37]. The criterion for representative plasma production makes it possible to measure thermal diffusivity because the mass entrained into the plasma plume is governed by the thermal diffusivity of the specimen. The total mass contained in the LPP plume, when measured, gives rise to a measure of the local thermal diffusivity [6]. We have further shown that the mass loss can be measured either by the impulse imparted on the target [5, 6, 36] or by time-resolved spectroscopy of the LPP plume [32, 33].

The total mass removed from the surface is determined by a number of competing processes: surface heating; phase transitions leading to vapor production; dispersal of the plasma matters by diffusion and hydrodynamic processes; and thermal diffusion into the bulk. These competing processes have been parameterized by three physical attributes of the constituent players in the form of a scaling relationship [6, 35–37]:

$$\theta = C D_{\mathrm{T}}^{\alpha} M^{\beta} H_{\mathrm{f}}^{\gamma}. \tag{1}$$

Here θ denotes the thickness of the LPP ablated layer in cm, D_{T} is the thermal diffusivity in units of $\mathrm{cm}^2 \cdot \mathrm{s}^{-1}$, M is the molar weight, and H_{f} is the heat of formation in $\mathrm{J} \cdot \mathrm{g}^{-1}$. $\mathrm{C} = 11.07 \pm 0.45$, $\alpha = 0.91 \pm 0.01$, $\beta = -\alpha$, and $\gamma = -1$. In determining the ablation layer thickness υ, it has been assumed that the layer has the mass density of the bulk. In cases where the

near-surface layers exhibit a significant depth dependence, it is best represented in terms of mass loss, m_{loss}: $m_{\text{loss}} = A\rho v$, where ρ is the bulk mass density and A denotes the area of the LPP ablation crater.

3. SPECTRAL EMISSION FLUX AND ELEMENTAL COMPOSITION OF 80–20 NICHROME RIBBON

The experimental setup is built around a small vacuum chamber consisting of a fused quartz cylinder. The vacuum chamber can be pumped down to a mid-10^{-6} Torr range. The specimen in the form of an 80–20 nickel-chromium ribbon is mounted on a metal flange on one end, and a large-diameter fused quartz lens is mounted on the opposite end. The laser beam and the detectors share the same lens by means of a dichroic mirror, which reflects the laser pulse but transmits the LPP plume emissions over the entire spectral range from near infrared to deep uv. The ribbon specimen has a thickness of 0.20 mm, and is 4.76 mm wide and 45.09 mm long. It is heated by ohmic heating up to 1300 K in temperature.

The glowing surface of the nickel-chromium ribbon is imaged onto a gated CCD array detector with 1024 by 256 detector pixels. The LPP plume is examined for elemental composition by means of time- and space-resolved spectroscopy at the same time. Such spectroscopic analyses are repeated to obtain the depth-resolved near-surface elemental composition profile. The accumulated mass loss after a number of LPP ablations is independently measured with a digital microbalance to provide a calibration for the mass loss measurement. Once the calibration has been carried out, it is possible to measure the thickness of the LPP ablation by spectroscopy without making physical contact with the specimen.

The heated surface, imaged with the white-light continuum emissions, was examined for the intensity distribution after each LPP ablation. After the first LPP ablation, the intensity of the crater area was reduced by 16.3%. When LPP ablation was continued in rapid succession, the intensity reduction leveled off at 40% below that of the undisturbed surrounding area. The initial intensity drop following the first LPP ablation can be understood simply enough as arising from the change in the elemental composition of the topmost layer. The LPP analysis showed it to be enriched with chromium, and the loss of the first ablation layer had an effect of reducing the chromium concentration. The specimen contains only two elemental species–namely, chromium and nickel, and their respective spectral emissivity values differ by less than 10%, chromium having the higher emissivity value. The continued decrease by as much as 40% is therefore not readily explained by the changing elemental composition alone.

Continued observation of the thermal emission intensity under a constant heating condition (at 1090 K) has revealed that the freshly exposed surface slowly recovers in thermal emission intensity over the next several minutes. Having learned that chromium is actively involved in the dynamics of the thermal radiation, we continued heating of a fresh Nichrome ribbon specimen at constant power for as long as 15 hours in a vacuum. The heated Nichrome ribbon was found to lose mass while the enrichment of chromium at the surface continued. This provided an opportunity to measure the surface temperature of the heated Nichrome ribbon. The rate of evaporation of nickel is several orders of magnitude lower than that of chromium. By attributing the evaporative loss rate of the heated Nichrome ribbon entirely to chromium evaporation, we were able to extract the temperature of the Nichrome ribbon from the rate of evaporation of chromium. The details of this technique are described elsewhere [34].

The surface of the aged specimen was then analyzed at room temperature in comparison with a fresh specimen. The final tabulation of layer-by-layer mass loss and elemental composition is summarized for the two specimens in Fig. 1. Figures 1a and 1b show the weight percent of the two elements for the fresh Nichrome specimen and the thickness of each ablation layer in μm, both as a function of depth from the specimen surface. Figures 1c and 1d show the corresponding results for the aged specimen. The conversion of the mass loss data into the thickness loss is accomplished by using the calculated local mass density of the alloy from the measured elemental composition in weight percent, the mass density of each constituent element, and the cross-sectional area of LPP ablation. The depth is obtained from the cumulative sum of the thickness losses.

A close examination of the LPP plume spectra from the fresh Nichrome ribbon shows that the topmost layer of the fresh specimen is enriched in chromium to a level slightly above that of the average concentration. This layer is, however, very thin such that the bulk composition emerges after only one or two LPP ablations. On the other hand, the aged specimen has developed a much thicker enriched chromium layer. In fact, the thickness of the transition region has been enlarged by a factor of three or more in 15 hours of heating at 1090 K. In view of the fact that the coefficient of diffusion is dependent on both the elemental mass and temperature, we expect that both the thermal history and local elemental composition contribute to the degree to which the near-surface composition profile is driven away from the uniform bulk composition. It follows naturally that the thermal diffusivity profile is modified as a result of such evolution of the near-surface composition profile, according to the scaling relationship given by Eq. (1).

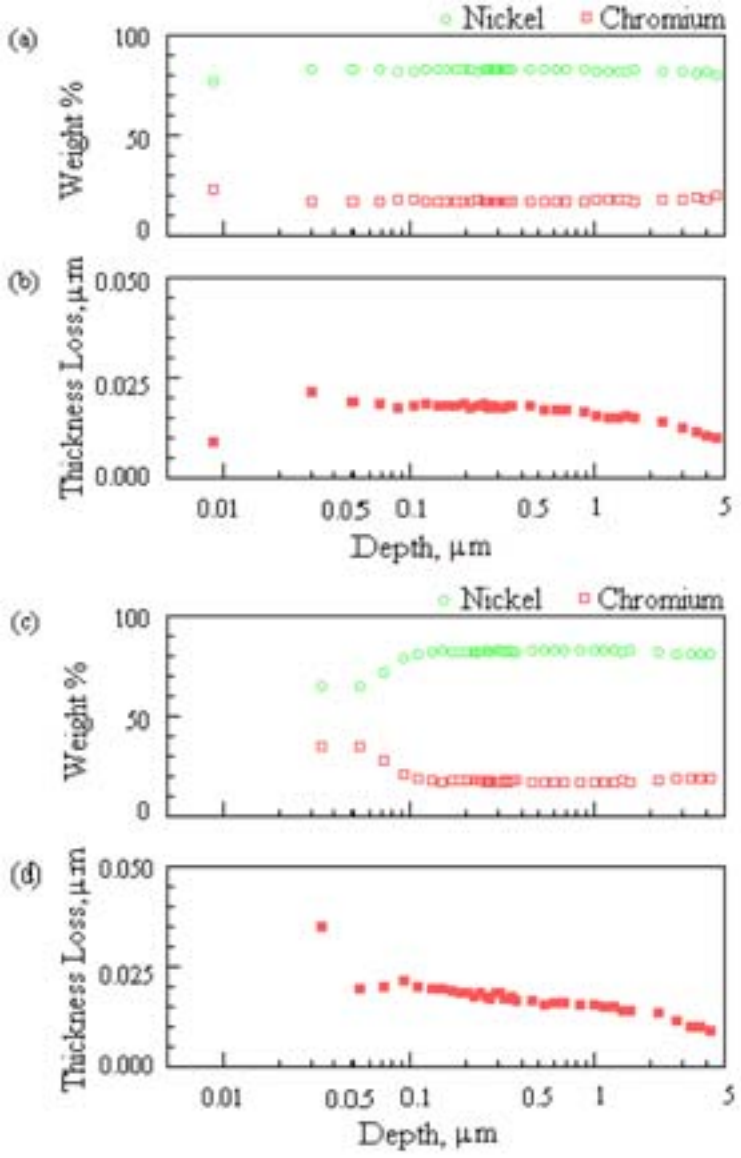

Fig. 1. Measured elemental composition and thickness of the ablation layer are plotted as functions of depth from the Nichrome ribbon surface at the outset of LPP plume analysis. A fresh Nichrome ribbon [(a) and (b)] is compared against a ribbon specimen aged by 15 h heating at 1090 K [(c) and (d)]. Open circles show the weight percent of nickel while open squares indicate that of chromium.

4. COMPOSITION PROFILE OF MAGNETIC "MUMETAL" SPECIMEN

In order to establish further the universal occurrence of nonuniform near-surface elemental composition profiles, independent of elemental composition, we have examined a magnetic "Mumetal" specimen for mass loss by LPP excitation and elemental composition. The specimen was prepared from 254 μm sheet stock with the following bulk concentration (in weight percent) of nickel, iron, copper, and molybdenum: 77:14:5:4. The resulting spectra are summarized in Fig. 2, which displays the emission spectrum obtained from a selection of 301 successive LPP plumes. Figure 2a displays the spectra as a spectrographic image. They reveal the now familiar trend. Several emission lines begin prominently at first but fade away in the succeeding LPP spectra, while the remainder asymptotically approach the spectrum representative of the bulk composition. Those fast fading emission lines turn out to be due to calcium residues of some unknown origins.

Figures 2b and 2c show the elemental composition and thickness loss, respectively, for each LPP excitation plotted against depth from the starting surface of the LPP analysis. The thickness loss per laser excitation has been deduced according to the procedure described for the Nichrome ribbon study, using the measured total mass loss of 133.7 ± 2.5 μg after 301 laser excitations as a calibration.

5. SURFACE COMPOSITION MODIFICATION OF WOOD'S ALLOY

We have carried out an experiment with four-element Wood's alloy of 50Wt% bismuth, 25Wt% lead, 12.5Wt% cadmium and 12.5Wt% tin. A specimen was melted in a sealed Pyrex crucible at 363 K, soaked at 363 K for 100 min, and then cooled over a period of 15 min. The top and bottom surface layers were examined by the method of LPP plume analysis. The two sets of spectra are shown in Fig. 3, one set of 29 spectra being from the bottom surface of the specimen and another set of 19 spectra from the top surface.

Figure 4 is a compilation of the elemental composition and mass loss per LPP ablation for the bottom surface (a) and the top surface (b) of the specimen, which have been deduced from the LPP plume spectra of Fig. 3. Figure 4 shows noticeably larger concentrations of lead and tin at the bottom surface of the specimen than at the top. It demonstrates the effect of symmetry breaking by the presence of gravity on the development of the composition profile throughout the Wood's alloy specimen. The data also

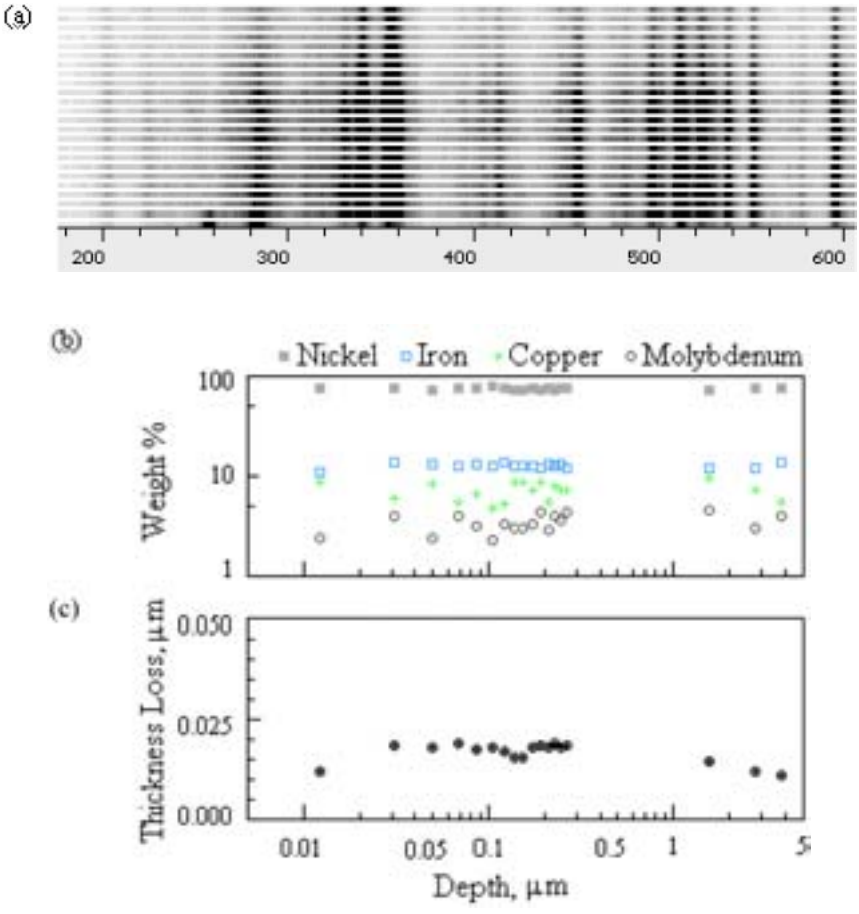

Fig. 2. A set of 24 emission spectra is shown of LPP plumes from a Mumetal specimen in gray-scale spectrogram format (a). The weight percent of nickel (filled square), iron (open square), copper (cross), and of molybdenum (open circle) are shown in logarithmic scale as a function of cumulative depth, also in logarithmic scale, from the starting surface of the Mumetal foil specimen (b). The thickness of the ablation layer removed by LPP excitation is also shown as a function of depth in logarithmic scale (c). The set of spectra is composed of those from the first fifteen successive LPP excitations in the order going from the bottom to the top, followed by the three clusters of three consecutive spectra, each cluster starting at the 99th, 199th, and 299th LPP ablation. The four elements of the alloy, nickel, molybdenum, iron, and copper, are tracked by the respective emission lines for elemental composition determination: 4714.42 Å NiI (pixel #856) for nickel; 4434.95 Å MoI (pixel #637); 4063.594 Å FeI (pixel #356) for iron; and 4032.647 Å CuI (pixel #332). Calcium impurity lines, 3933.666 Å CaII (pixel #259), 3968.468 Å CaII (pixel #286) and 4226.728 Å CaI (pixel #478), rise and fade within the first two LPP ablations.

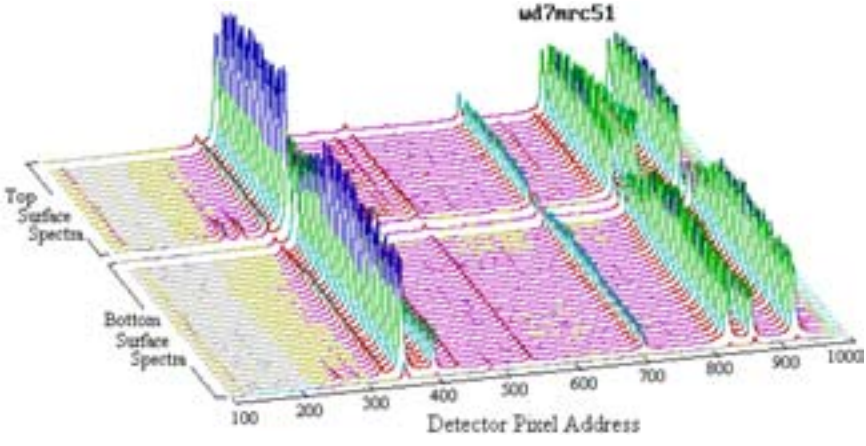

Fig. 3. The LPP plume emission spectra from the top and bottom surfaces of a Wood's alloy specimen, which had been melted and resolidified according to a protocol described in the text. The first twenty-nine spectra of the LPP plume emissions starting from the lower end of the figure are obtained from the bottom surface of the solidified specimen and the last nineteen spectra are from the top surface. The 29th spectrum of the bottom group is taken from a surface 1.14 mm below the bottom surface, whereas the 19th of the top group is taken at a depth of 0.51 mm from the top surface.

show that the manner in which the elemental concentration varies with depth is different for the top surface from that for the bottom surface.

The two sets of mass loss data also compare the thermal diffusivity profile at the bottom surface (Fig. 4a) of the Wood's alloy specimen to that of the top surface (Fig. 4b) of the same specimen. At a first glance it is tempting to conclude that the thermal diffusivity is significantly higher at the top surface than at the bottom. A closer examination of the mass loss data suggests caution. The composition profiles of the two surfaces converge toward each other after a large number of ablations but the mass loss data remain significantly higher for the top surface than for the bottom surface.

Recall that Eq. (1) quantifies the roles of thermal diffusion (D_T), the heat of formation (H_f), and thermal motion (M) of the free elemental species in determining the amount of mass lost during a LPP ablation. We have a firm grasp of both the amount of target mass entrained into the LPP plume and the elemental composition of the plume. The thermal velocity distribution of the constituent species in the plume is also well prescribed. The heat of formation of the species that had resided within the ablation layer of the specimen's surface is, however, affected by both the atomic properties and the morphology within the alloy layer. It is the

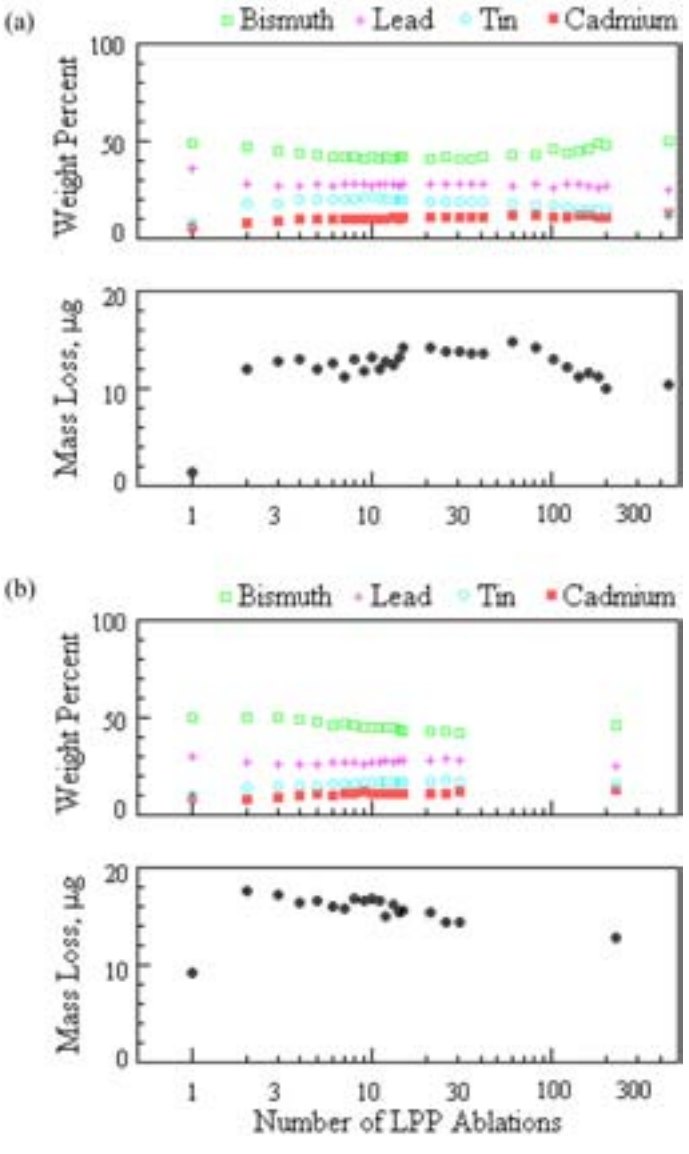

Fig. 4. Measured elemental concentration and mass loss for a Wood's alloy specimen. The results are derived from the set of spectra shown in Fig. 3. The data from the bottom surface of the specimen are shown in (a) and those from the top surface are presented in (b). The following emission lines are used: 4057.807 Å PbI (pixel #352) for lead; 4524.74 Å SnI (pixel #706) for tin; 4722.52 Å BiI (pixel #863) for bismuth; and 4678.149 Å CdI (pixel #827) and 4799.912 Å CdI (pixel #925) for cadmium.

morphology that is subject to some interpretation. It is quite conceivable that the defect densities of the two surface layers may differ to an extent that is nontrivial. The common way of estimating the heat of formation of multi-element alloy presumes that elemental constituents exist as densely packed elemental clusters within the alloy medium. The morphology issue may force an alternative approach to such an estimate. In the absence of any independent method of including the morphology contribution, the heat of formation remains uncertain by an unknown amount, and therefore we present the mass loss as a best measure of the depth dependence of thermal diffusivity at present.

While the elemental compositions of the individual ablation layers have been fully characterized, no independent determination of the changes in the morphology of the ablation layer has been attempted. Morphology characterization of a material specimen is a difficult task. The kind of thermal diffusivity analysis presented in this paper may, in fact, help quantify the morphology once the composition effects in the development of the thermal diffusivity profile have been reasonably accounted for.

6. SUMMARY AND CONCLUSIONS

We have examined three different alloy systems–namely, two-element Nichrome, four-element Mumetal, and four-element Wood's alloy, by the method of time- and space-resolved spectroscopy of LPP plumes. Each of them has revealed the presence of a near-surface elemental composition profile that is nonuniform in nanometer scale and significantly different from the bulk composition. They add to the growing body of evidence that such a nonuniform composition profile is universal and intrinsic to the fact that solid specimens have free surfaces. Depth-resolved mass loss measurements clearly demonstrate the cause and effect relationship between thermophysical properties of a given material and its local elemental composition profile. The sensitivity to the local composition profile is particularly strong for spectral emissivity. Because of large thermal fluctuations within the material specimen at elevated temperatures, the near-surface composition profile evolves over time, and this, in turn, imposes the time dependent nature to specific emissivity in particular and the thermophysical properties in general.

The thickness of the ablated surface layer that have been presented in Figs. 1, 2, and 4 can be converted into depth-resolved thermal diffusivity of the respective specimens by use of the scaling relationship of Eq. (1). Any nonuniformity in the thickness loss data and elemental composition leads to a nonuniform profile of local thermal diffusivity. By the same token, any temporal movement of the elemental composition profile will result in a time-dependent thermal diffusivity profile.

We have also shown that the thickness of the near surface region over which elemental composition changes significantly can be modified substantially by altering the thermal history of melting-resolidification cycle. The study with the Wood's alloy specimen underscores this point dramatically. It appears highly likely that widely varying values in the thermophysical reference data [38–43] may be traceable, in part, to the variability in the near-surface elemental composition profile of a given material specimen used in each measurement, as a contributing factor. In our extended exploration with the method of LPP plume spectroscopy, we have found that no specimens, not even the reagent-grade pure elemental specimens, exhibit uniform near-surface composition profiles. Trace-level impurities in pure specimens percolate to the surface to modify the composition of near-surface layers.

In the absence of any effective means for control of near-surface elemental composition profiles, the next best approach is to fully characterize the composition profile whenever basic thermophysical properties are measured. The LPP plume spectroscopy method is an effective tool to satisfy the dual goal of measurement and characterization.

The fact that LPP plume spectroscopy exposes the surface of a specimen one ablation layer after another has led to a serendipitous observation about the heated specimen. In the case of the electrically heated Nichrome ribbon, the white light emission intensity can decrease by as much as 40% when the surface is ablated repeatedly. In view of the measured composition of the local surface layer, this decrease is too large to be explained by a decrease in spectral emissivity alone. Rather, it is necessary to recognize the existence of a negative temperature gradient at the surface, which may be of the order of a five-percent drop in temperature over 15 ablation layers. A detailed analysis of the heating and loss rates point to the role of a nonuniform electrical resistivity profile in the thermal balance [34]. As such, it too is affected by the elemental composition profile.

ACKNOWLEDGMENT

This work was supported in part by the CTU 5–2 Consortium on Laser-Produced Plasmas and Lehigh University.

REFERENCES

1. F. Righini, J. Spisiak, and G. C. Bussolino, *Int. J. Thermophys.* **20**:1095 (1999).
2. S. Krishnan and P. C. Nordine, *J. Appl. Phys.* **80**:1735 (1996).
3. J. G. Na, *J. Vac. Sci. Technol. A* **13**:2739 (1995).
4. J. M. E. Harper, C. Cabral, Jr., P. C. Andricacos, L. Gignac, I. C. Noyan, K. P. Rodbell, and C. K. Hu, *J. Appl. Phys.* **86**:2516 (1999).

5. Y. W. Kim, *Int. J. Thermophys.* **20**:1313 (1999).
6. Y. W. Kim, in *Thermal Conductivity 25/Thermal Expansion 13*, C. Uher and D. Morelli, eds. (Technomic Publishing, Lancaster, Pennsylvania, 2000), p. 15.
7. W. H. Hofmeister, M. B. Robinson, and R. J. Bayuzick, *Appl. Phys. Lett.* **49**:1342 (1986).
8. B. T. Bassler, W. H. Hofmeister, R. J. Bayuzick, R. Gorenflo, T. Bergman, and L. Stockum, *Rev. Sci. Instr.* **63**:3466 (1992).
9. B. T. Bassler, R. S. Brunner, W. H. Hofmeister, and R. J. Bayuzick, *Rev. Sci. Instr.* **68**:1846 (1997).
10. P. Liu, L. L. Sun, J. H. Zhao, X. Y. Zhang, D. W. He, Z. C. Qin, Y. F. Xu, and W. K. Wang, *Appl. Phys. Lett.* **71**:64 (1997).
11. G. W. Young and H. Davis, *Phys. Rev. B* **34**:3388 (1986).
12. D. N. Riahi, *Phys. Fluids A* **3**:2816 (1991).
13. D. A. Huntley and S. H. Davis, *Phys. Rev. B* **53**:3132 (1996).
14. B. Robinson, D. Li, J. R. Rogers, R. W. Hyers, L. Savage, and J. Rathz, *Appl. Phys. Lett.* **77**:3266 (2000).
15. I. Egry, G. Lohoefer, and G. Jacobs, *Phys. Rev. Lett.* **75**:4043(1995).
16. L. M. Racz and I. Egry, *Rev. Sci. Instr.* **66**:4254 (1995).
17. M. Perez, L. Salvo, M. Suéry, Y. Bréchet, and M. Papoular, *Phys. Rev. E* **61**:2669 (2000).
18. M. Conti, *Phys. Rev. E* **55**:701 (1997).
19. M. Conti, *Phys. Rev. E* **55**:765 (1997).
20. M. Conti, *Phys. Rev. E* **56**:3717 (1997).
21. M. Conti, *Phys. Rev. E* **19**:642 (2000).
22. G. Giacomin and J. L. Lebowitz, *Phys. Rev. Lett.* **76**:1094 (1996).
23. J.-M. Liu, L. C. Lim, and Z. G. Liu, *Phys. Rev. B* **60**:7113 (1999).
24. C. A. Laberge, P. Fratzl, and J. L. Lebowitz, *Phys. Rev. Lett.* **75**:4448 (1995).
25. V. I. Gorentsveig, P. Fratzl, and J. L. Lebowitz, *Phys. Rev. B* **55**:2912 (1997).
26. P. Maugis, *Phys. Rev. B* **53**:5276 (1996).
27. J.- M. Liu, *J. Appl. Phys.* **84**:6582 (1998).
28. H. Reichert, P. J. Eng, H. Dosch, and I. K. Robinson, *Phys. Rev. Lett.* **74**:2006 (1995).
29. Y. Yang, K. A. Nelson, and F. Adibi, *J. Mater. Res.* **10**:41 (1995).
30. S. De Panfilis and A. Filipponi, *J. Appl. Phys.* **88**:562 (2000).
31. Y. W. Kim, in *Laser-Induced Plasmas and Applications*, L. J. Radziemski and D. A. Cremers, eds. (Marcell Dekker, New York, 1989), Chap. 8.
32. Y. W. Kim, *High Temp. Sci.* **26**:57 (1990).
33. Y. W. Kim, U.S. Patent Number 4, 986, 658 (22 January 1991).
34. Y. W. Kim, *Int. J. Thermophys.* (in press).
35. Y. W. Kim, *Int. J. Thermophys.* **14**:397 (1993).
36. Y. W. Kim and C.-S. Park, *Int. J. Thermophys.* **17**:713 (1996).
37. Y. W. Kim and C.-S. Park, *Int. J. Thermophys.* **17**:1125 (1996).
38. D. E. Gray, ed., *AIP Handbook*, 3rd Ed. (McGraw–Hill, New York, 1972).
39. W. E. Forsythe, *Smithsonian Physical Table*, 9th Ed. (The Smithsonian Institution, Washington, 1954).
40. W. M. Rohsenow, J. P. Hartnett, and Y. I. Cho, *Handbook of Heat Transfer*, 3rd Ed. (McGraw–Hill, NY, 1998), Chap. 16.
41. H. E. Boyer and T. L. Gall, eds., *Metals Handbook* (ASM, Metals Park, Ohio, 1985).
42. D. L. Lide, ed., *Handbook of Chemistry and Physics*, 75th Ed. (CRC Press, Boca Raton, Florida 1994).
43. Y. S. Touloukian, et al., *Thermophysical Properties of Matter*, Vol. 1–3 (IFI/Plenum, New York, 1970–1975).